catalysts

MDPI

Article

Response Surface Methodology and Aspen Plus Integration for the Simulation of the Catalytic Steam Reforming of Ethanol

Bernay Cifuentes, Manuel Figueredo and Martha Cobo *

Energy, Materials and Environment Laboratory, Department of Chemical Engineering, Universidad de La Sabana, Campus Universitario Puente del Común, Km. 7 Autopista Norte, Bogotá 250001, Colombia; bernayciva@unisabana.edu.co (B.C.); manuel.figueredo@unisabana.edu.co (M.F.)

* Correspondence: martha.cobo@unisabana.edu.co; Tel.: +571-8615555 (ext. 25207); Fax: +571-8615555

Academic Editor: Simon Penner

Received: 20 November 2016; Accepted: 27 December 2016; Published: 14 January 2017

Abstract: The steam reforming of ethanol (SRE) on a bimetallic RhPt/CeO_2 catalyst was evaluated by the integration of Response Surface Methodology (RSM) and Aspen Plus (version 9.0, Aspen Tech, Burlington, MA, USA, 2016). First, the effect of the Rh–Pt weight ratio (1:0, 3:1, 1:1, 1:3, and 0:1) on the performance of SRE on RhPt/CeO_2 was assessed between 400 to 700 °C with a stoichiometric steam/ethanol molar ratio of 3. RSM enabled modeling of the system and identification of a maximum of 4.2 mol H_2/mol EtOH (700 °C) with the $Rh_{0.4}Pt_{0.4}/CeO_2$ catalyst. The mathematical models were integrated into Aspen Plus through Excel in order to simulate a process involving SRE, H_2 purification, and electricity production in a fuel cell (FC). An energy sensitivity analysis of the process was performed in Aspen Plus, and the information obtained was used to generate new response surfaces. The response surfaces demonstrated that an increase in H_2 production requires more energy consumption in the steam reforming of ethanol. However, increasing H_2 production rebounds in more energy production in the fuel cell, which increases the overall efficiency of the system. The minimum H_2 yield needed to make the system energetically sustainable was identified as 1.2 mol H_2/mol EtOH. According to the results of the integration of RSM models into Aspen Plus, the system using $Rh_{0.4}Pt_{0.4}/CeO_2$ can produce a maximum net energy of 742 kJ/mol H_2, of which 40% could be converted into electricity in the FC (297 kJ/mol H_2 produced). The remaining energy can be recovered as heat.

Keywords: Aspen-Plus; bimetallic Rh-Pt; hydrogen; Response Surface Methodology; steam reforming

---

1. Introduction

At the Framework Convention on Climate Change (COP21) of the United Nations (UN) held in Paris in 2015, the urgency of global replacement of fossil fuels by renewable energy sources was raised [1]. This has promoted the development of engineering projects related to sustainable fuels. Particularly, the production of electricity in fuel cells (FC) fed with hydrogen (H_2) is an interesting energy model: the process does not generate pollution, and it can be implemented in several mobile and stationary applications [2]. Currently, most H_2 is produced from non-renewable resources such as natural gas, but biomass has been proposed as a sustainable source for H_2 production. Particularly in Colombia, bioethanol, a fuel obtained from biomass, has emerged as a promising resource for H_2 production due to the thermodynamic favorability of its reformation [3] and its increased production in recent years through Colombian government promotion [4]. Currently, bioethanol is blended with gasoline (8–10 vol %) in transport applications. However, the use of ethanol/gasoline mixtures in internal combustion engines leads to low volumetric efficiencies (<48%) and generates pollution [5]. Otherwise, the conversion of ethanol to H_2 could give added value to bioethanol production and promote new business in Colombia.

H_2 production from ethanol may be carried out by steam reforming of ethanol (SRE). This method has the advantage of producing a greater amount of H_2 per mole of ethanol [6], and it is more economical compared to other methods, such as partial oxidation, auto-thermal reforming, or oxidative steam reforming [6–8]. SRE is an endothermic process (347 kJ/mol) [9] that involves a network of chemical reactions (Table 1, [10–12]). Depending on the reaction conditions, the nature of the support, and the active phase, different routes can take place to produce a complex set of products, including H_2, carbon monoxide (CO), methane (CH_4), carbon dioxide (CO_2), ethane (C_2H_6), ethylene (C_2H_4), and acetaldehyde (CH_3CHO) [13,14].

Table 1. Network of chemical reactions during the steam reforming of ethanol [10–12].

Reaction	Description	
$CH_3CH_2OH + 3H_2O \rightarrow 2CO_2 + 6H_2$	(Steam reforming–ethanol)	Equation (1)
$CO + H_2O \rightleftharpoons CO_2 + H_2$	(Water gas shift reaction)	Equation (2)
$CH_3CH_2OH \rightleftharpoons CH_3CHO + H_2$	(Dehydrogenation–ethanol)	Equation (3)
$CH_3CH_2OH \rightleftharpoons C_2H_4 + H_2O$	(Dehydration–ethanol)	Equation (4)
$CH_3CH_2OH \rightleftharpoons CH_4 + CO + H_2$	(Decomposition–ethanol)	Equation (5)
$CH_3CHO \rightleftharpoons CH_4 + CO$	(Decomposition–acetaldehyde)	Equation (6)
$CH_3CHO + H_2O \rightleftharpoons CH_4 + CO_2 + H_2$	(Steam reforming–acetaldehyde)	Equation (7)
$CH_4 + H_2O \rightleftharpoons CO + 3H_2$	(Steam reforming–methane)	Equation (8)
$2CH_4 \rightleftharpoons C_2H_4 + 2H_2$	(Dehydrogenation–methane)	Equation (9)
$C_2H_4 + 4H_2O \rightleftharpoons 2CO_2 + 6H_2$	(Steam reforming–ethylene)	Equation (10)

Base metals, such as Ni [15], Co [16], and Fe [17], and noble metals, such as Pd [18], Rh [18,19], Pt [7,20], and Ir [21], supported on metals oxides to catalyze SRE have been widely studied. The nature of the catalyst and operational conditions directly affect its performance in SRE [15,22]. Ni is a widely studied catalyst due to its low cost [10]. However, Ni promotes the formation of carbonaceous species, and it has low stability [23]. In contrast, noble metals are promising candidates for SRE because of their higher activity and stability with a low formation of coke [24]. Among the noble metals, Rh catalysts showed better performance in terms of conversion of ethanol and H_2 production [25], even at low catalyst loadings (<1 wt %) [26]. However, Rh promotes ethanol dehydrogenation with high CO formation (Equations (3) and (6)) [18]. On the contrary, Pt favors CO adsorption on the catalyst surface and affects reducible species on the support, promoting the formation of new active sites in the water gas shift reaction (WGSR) [27,28]. Yet, Pt has a lower capacity to break C–C bonds compared to Rh [29]. Therefore, the development of bimetallic structures that are simultaneously active in the two reactions is desirable [30,31].

In our previous work, a bimetallic 0.6 wt % Rh–0.2 wt % Pt over CeO_2 catalyst appeared to have a high activity in SRE and WGSR with a low susceptibility to coke formation [32]. The main drawback of this catalyst is its high cost. Hence, high stability and activity with low metal loadings are required. Furthermore, the noble metals ratio in the catalyst possibly has an effect on the catalytic performance. Idriss et al. [33] reported that the Pd–Rh ratio affects the selectivity and activity of a $RhPd/CeO_2$ catalyst in SRE and that a minimum load of active metals could be required to improve H_2 production. Kaila et al. [34] evaluated a bimetallic $RhPt/ZrO_2$ in the autothermal reforming of simulated gasoline, reporting that CH_4 reforming was altered by the Rh–Pt ratio due to the formation of different Rh_xPt_{1-x} alloys in $RhPt/ZrO_2$. Therefore, the Rh–Pt ratio could have an impact on the catalyst performance of $RhPt/CeO_2$ catalysts for SRE, not only on the H_2 yield but also on the energy efficiency of the process.

Analysis of catalytic performance and energy efficiency is a decisive step in the implementation of a large-scale process [35]. Innovative methodologies and commercial software are widely used in process assessment. The Response Surface Methodology (RSM) is a powerful tool to evaluate processes because it allows for the determination of the effect of multiple variables on an interest response [36]. This technique is widely used in industrial assessments and research projects. Nevertheless, in some areas of chemistry and chemical engineering, RSM is poorly used. Recently, the use of RSM in catalysis for the evaluation of catalysts and process optimization was reported [37,38]. RSM allows for direct predictions about the performance of a process in a particular region from experimental data. Moreover, this information can be fed to commercial software for further analysis of the process. Aspen Plus is a widely used software for the simulation of H_2 production from steam reforming. For instance, Rossetti et al. [39] quantified electrical power, thermal energy output, and overall efficiency of a plant based on SRE. Genyin et al. [40] created a user-defined model built in FORTRAN (version 9.0, Aspen Tech, Burlington, MA, USA, 2016) to simulate a fluidized bed membrane reactor for H_2 production. The main limitation of the simulator is that it requires detailed information on the kinetics of the process in order to adequately predict the experimental data. However, the RSM model can be integrated into Aspen Plus to combine both experimental and simulated data as a powerful tool for process assessment and improvement. Nevertheless, there are few works [41,42] which have integrated Aspen Plus and RSM, specifically in separation processes. Thus, no reports of Aspen Plus and RSM integration for the assessment of catalytic sustainable energy models or H_2 economy were found.

This study aimed to simulate SRE on a RhPt/CeO_2 catalyst, integrating RSM and Aspen Plus to determinate the effect of the Rh–Pt ratio on its further energy performance in FC. For this purpose, the effect of the Rh–Pt ratio in a bimetallic RhPt/CeO_2 catalyst on catalytic activity, H_2 yield, product distribution, energy requirements, and energy generation were evaluated by RSM and Aspen Plus. The use of response surfaces allowed the selection of a Rh–Pt ratio more suitable for obtaining active and selective materials for SRE. The mathematical models obtained from the RSM were integrated into Aspen Plus in order to simulate the power generation in FC.

2. Results and Discussion

2.1. Effect of the Rh–Pt Ratio on the Catalytic Performance

Table 2 shows the different Rh–Pt ratios evaluated for the RhPt/CeO_2 catalyst used in SRE. The experimental data shown as Appendix (Table A1) was used to obtain response surfaces of these catalytic materials from 400 to 700 °C. Response surfaces were plotted in Figure 1. The Rh axis shows the wt % Rh, but the total nominal metal loading (Rh + Pt) was always 0.8 wt % in all catalysts.

Table 2. RhPt/CeO_2 catalysts evaluated in steam reforming of ethanol (SRE).

Catalyst [1]	Rh (wt %)	Pt (wt %)	Rh–Pt (wt ratio)	Weight Loss of Used Catalyst Samples (mg carbon/(g_{cat}·h)) [2]
CeO_2	0	0	0:0	4.06
$Rh_{0.8}/CeO_2$	0.8	0	1:0	1.00
$Rh_{0.6}Pt_{0.2}/CeO_2$	0.6	0.2	3:1	0.36
$Rh_{0.4}Pt_{0.4}/CeO_2$	0.4	0.4	1:1	0.42
$Rh_{0.2}Pt_{0.6}/CeO_2$	0.2	0.6	1:3	0.52
$Pt_{0.8}/CeO_2$	0	0.8	0:1	3.31

[1] Subscripts in RhPt/CeO_2 catalysts correspond to the nominal metal loading; [2] measured by thermogravimetric analysis (TGA).

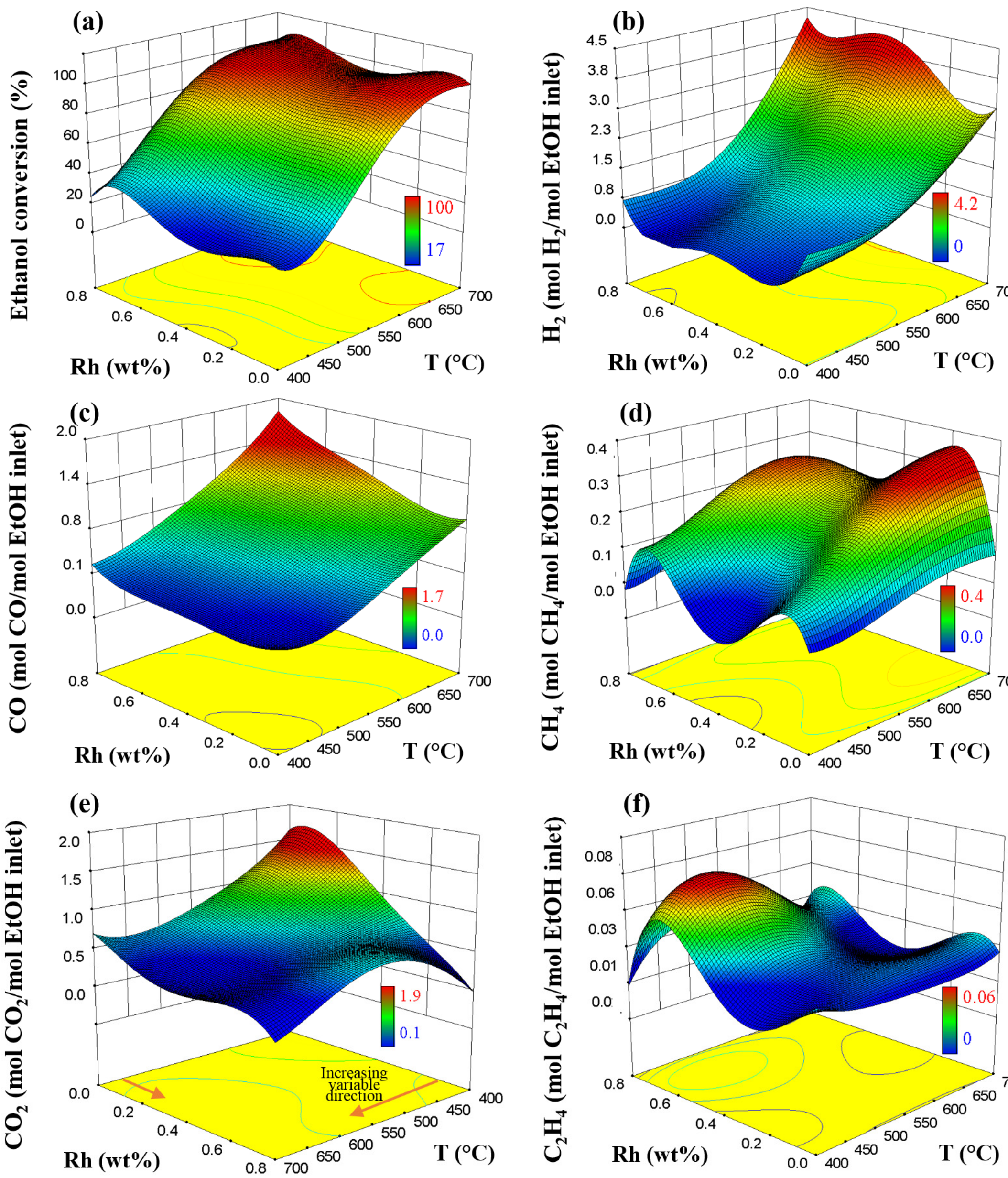

Figure 1. (**a**) Ethanol conversion (X_{EtOH}) and yields of (**b**) H_2, (**c**) CO, (**d**) CH_4, (**e**) CO_2, and (**f**) ethylene (C_2H_4) as a function of temperature over $RhPt/CeO_2$ with different Rh–Pt ratios. Total metal loading (Rh + Pt) = 0.8 wt % in all catalysts. Response surface: Quartic model, $R^2 > 0.85$, Adjusted $R^2 > 0.82$, *Probability F* << 0.1 (significant), and *Lack of Fit* >> 3 (nonsignificant). Reaction conditions: $S/E = 3$, 100 mg catalyst, and $GHSV$ = 70,600 h^{-1}. Arrows in Figure 1e show the increasing variable direction.

SRE is favored by temperature (Figure 1a) due to its endothermic character. This effect is exponential, and complete ethanol conversion is ensured above 600 °C under the current conditions. Some values of the RSM appeared slightly higher than 100% ethanol conversion due to a slight deviation from the actual data by the adjustment of the mathematical model ($R^2 < 1$). The $Rh_{0.7}Pt_{0.1}/CeO_2$ catalyst showed more activity, reaching total ethanol conversion above 560 °C (Figure 1a). Rh has been identified as the most active catalyst for ethanol conversion in SRE due to the lower intrinsic activation barrier of Rh catalysts, which favors the C–C bond dissociation [43]. A significant effect of the Rh–Pt ratio on H_2 yield was identified (Figure 1b). A decrease in H_2 yield was observed when low Rh loadings were present (0–0.2 wt %). From this point, a maximum of

4.2 mol H_2/mol EtOH (700 °C) was obtained with the $Rh_{0.4}Pt_{0.4}/CeO_2$ catalyst, which is 8% and 25% more compared to monometallic Rh/CeO_2 and Pt/CeO_2, respectively. The presence of Rh in the bimetallic catalyst has been linked to a better ability to break C–C bonds and reform CH_4 [18,23] (Equations (3) and (8)), favoring H_2 production. Below 520 °C, $Pt_{0.8}/CeO_2$ showed a higher H_2 yield. Pt favors CO adsorption on the catalyst surface and affects the reducible species on the support [13], promoting H_2 production by WGSR [28,44] (Equation (2)), which is favored at low temperature because it is an exothermic reaction [45]. Rh would also slightly favor WGSR [46]. Hence, H_2 production at low temperatures is mainly by WGSR, which seems to be favored on the monometallic samples.

Figure 1c–f show the byproducts' yield during SRE. The higher the temperature and the Rh loading, the higher the CO production (Figure 1c). WGSR (Equation (2))—responsible for the CO control during the process—is favored at low temperatures (<500 °C) [45]. This reaction may occur through two mechanisms [47]: (i) a reaction between CO and OH^- species on the catalyst surface, with formate as the intermediate, to produce CO_2 (Equations (11) and (12)); and (ii) a direct oxidation with O_2 by the Eley–Rideal (E–R) mechanism with surface oxygen as the intermediate (Equation (13)). In both cases, the previous dissociation of water is required (Equation (14)).

$$OH^- + CO \rightleftharpoons OCOH \tag{11}$$

$$2OCOH \rightleftharpoons 2CO_2 + H_2 \tag{12}$$

$$O^+ + CO \rightleftharpoons CO_2 \tag{13}$$

$$H_2O \rightleftharpoons O^+ + OH^- \tag{14}$$

The oxygen storage capacity (OSC) of the support increases the favorability of the E–R mechanism [48]. Scarabello et al. [46] reported that the O-vacancy in $Rh/Ce\text{-}ZrO_2$ promotes the oxidation of CO to CO_2 by the reaction in Equation (15) and the dissociation of water, increasing H_2 production (Equation (16)). Thus, the high OSC of CeO_2 would help to promote the WGSR in $RhPt/CeO_2$ through E–R mechanisms. This model also explains the regeneration of O^- species in CeO_2 by the presence of water in SRE.

$$2CeO_2 + CO \rightleftharpoons CO_2 + Ce_2O_3 \tag{15}$$

$$Ce_2O_3 + H_2O \rightleftharpoons 2CeO_2 + H_2 \tag{16}$$

The active metal (M) can promote different reaction mechanisms in CO formation [49]. Liu et al. [50] studied CO oxidation over a Pt/CeO_2 catalyst. These authors proposed that the formation of a Pt–Ce–O solid solution accelerates the mobility of lattice oxygen and improves the oxidation of CO. Diagne et al. [51] reported that the formation of CO in SRE on Rh/CeO_2 followed the sequence: dehydrogenation of ethanol (Equation (3)) → acetaldehyde decomposition (Equation (6)) → CH_4 reforming (Equation (8)). In addition, the presence of Rh_2O_3 and RhO_2 species on the catalytic surface was reported. Likewise, Sheng et al. [19] informed that the presence of Rh in $RhPt/CeO_2$ can promote the formation of an oxametallacycle ($M_2\text{-}OCH_2CH_2$), which decomposes to CO and CH_4 at high temperatures. Cavallaro [52] reported that Rh-catalysts promoted steam reforming of CH_4 (Equation (8)) and ethylene (Equation (10)) at high temperatures. Then, the increase in the content of Rh in $RhPt/CeO_2$ catalysts favors the simultaneous production of CO and H_2. The close relationship between the Rh–Pt ratio, H_2 yield, and CO production would affect the energy requirements of the electricity production by FC due to the fact that the FC cannot be fed by H_2 streams with CO concentrations larger than 10 ppm [53].

On the other hand, CH_4 is an undesirable byproduct because it decreases the H_2 yield. CH_4 production increased between 400 and 600 °C (Figure 1d). The decomposition of ethanol (Equation (5)) and slow CH_4 reforming (Equation (8)) could be taking place [26,54]. Above 600 °C, complete conversion of ethanol was ensured (Figure 1a), and a decrease in CH_4 production was observed in most of the catalysts (Figure 1d), except for $Rh_{0.2}Pt_{0.6}/CeO_2$. This is consistent with previous reports [46,55]. Also, previous investigations of the reaction mechanism of SRE over M/CeO_2 suggested that ethoxy-species and acetaldehyde are involved as intermediates in CH_4 formation [56,57]. Subsequently, the conversion of CH_4 to C1 species is expected at high temperatures [58]. Also, Rh- and Pt-supported catalysts are known for their ability to reform CH_4; this effect is improved by the presence of Ce^{n+} species on the support due to a synergetic contribution among M–Ce to cleave C–C bonds [46,59].

However, the bimetallic catalysts were less effective for reforming CH_4 compared to their monometallic counterparts (Figure 1d). Specifically, a greater amount of CH_4 formation was observed on $Rh_{0.2}Pt_{0.6}/CeO_2$ at high temperatures. In our previous work, Rh–Pt–Rh_2O_3 particles were reported as possible active sites in SRE, which favor the catalyst's high stability [26,32]. However, shortcomings of this catalyst to reform CH_4 at high temperatures were detected. Similarly, Kaila et al. [34] evaluated $RhPt/ZrO_2$ catalysts with different Rh–Pt ratios in autothermal reforming of simulated gasoline (*steam*/*carbon* = 3, 0.5 wt % total metal loading, 400–900 °C), reporting that the Rh–Pt ratio affected the product distribution due to Rh_xPt_{1-x} alloy formation. At 700 °C, $Rh_{0.1}Pt_{0.4}/ZrO_2$ presented the lowest concentration of CH_4 (0.2 mol %) compared to the other catalysts. In this work, $Rh_{0.4}Pt_{0.4}/CeO_2$ showed the least amount of CH_4 among the bimetallic catalysts (Figure 1d), which could explain the higher H_2 yield for this catalyst (Figure 1b). As discussed in our previous work [32,37], evidence of Rh–Pt alloy formation was found on the $RhPt/CeO_2$ catalysts. Thus, Rh–Pt alloy formation on $RhPt/CeO_2$ catalysts promotes different product distributions depending on the Rh–Pt ratio.

CO_2 is an indicator of the WGSR presence (Equation (2)) in SRE [44,51]. The increased formation of CO_2 (Figure 1e) was detected at low temperatures (<560 °C) on the catalysts with higher Pt content (0.2–0.4 wt % Rh), in which conditions the WGSR was favored. This also explains the low CO formation in this zone (Figure 1c), as previously discussed. Diagne et al. [48] proposed that CH_4 reforming is followed by WGSR over Rh/CeO_2 and Rh/CeO_2–ZrO_2, avoiding accumulation of CH_4 and CO in SRE. Therefore, the equilibrium reaction of CH_4 reforming (Equation (8)) would be favored by the presence of steam and the reduction in CO concentration through WGSR (Equation (2)) [60,61]. This could be consistent with the results obtained in this study, in which the formation of CH_4 and CO was lower at low temperatures. However, as the temperature rose and the WGSR was disfavored, the concentrations of CO and CH_4 increased.

Although ethylene is a known intermediate in SRE, low production of ethylene (Figure 1f) was observed as compared to CH_4, which is a more stable intermediate [10]. Zanchet et al. [62] reported that ethylene formation decreases on CeO_2 above 250 °C because of the energy barrier limit of ethanol dehydration (Equation (4)) and affects the stability of ethoxy intermediates, favoring dehydrogenation and decomposition reactions. This agrees with the results obtained in this work, in which ethylene production was very limited, decreasing with temperature. The effect of this ethylene production on the formation of carbonaceous species over the catalysts was measured by thermogravimetric analysis (TGA) (Table 2). The bimetallic catalysts ($Rh_xPt_{0.8-x}/CeO_2$) showed less formation of carbonaceous compounds compared to the monometallic samples (Rh/CeO_2 and Pt/CeO_2). The Pt content in the bimetallic catalysts increased the rate of weight loss. However, monometallic catalysts (Rh/CeO_2 and Pt/CeO_2) showed lower production of ethylene compared to bimetallic catalysts. It is accepted that Rh favors C–C dissociation [43] and that bimetallic Rh–noble metal on basic supports contributes to the mitigation of carbon deposition [18,32]. In addition, the presence of higher amounts of CO_2 on the bimetallic catalysts could be an indication of ethylene reforming (Equation (10)) [52]. Therefore, low ethylene formation in monometallic catalysts could be due to ethylene polymerization. Ethane and acetaldehyde were not detected for any catalyst, possibly due to the fact that noble metals accelerate the thermal cracking of such light hydrocarbons [23].

2.2. Models of the SRE from the RSM

The regression analysis and the Analysis of Variance (ANOVA) for the response surfaces are shown in Table 3. The R^2 > 0.9, the "*Probability F*" << 0.5 (significant), and the *Lack of Fit* >> 3 (nonsignificant) indicate that these models fit well to experimental data [63] and that they can be used to make predictions about the responses. The "*Coded Factors*" are useful for identifying the relative impact of the factors through comparison of the factor coefficients. Nonsignificant terms in the "*Coded Factors*" ("*Probability F*" > 0.1) indicate that this effect has no relevance to the response, and they were not included. Meanwhile, the "*Actual Factors*" of Table 3 can be used to make predictions about the response for given levels of each factor, replacing them in the quartic model shown in Equation (17). The mathematic model from the "*Actual Factors*" can be used for simulations in commercial software in order to obtain preliminary energy information about the process. Statistical parameters such as the "*Probability F*" << 0.5, *Lack of Fit* >> 3, and "*Adequate Precision*" > 4 show that the models fit well [63]. Nevertheless, some values deviate slightly from the actual data, such as ethanol conversion above 100%, due to the statistical error and the adjustment of the mathematical model (R^2 < 1). All the experimental values employed to obtain the response surfaces were included as Appendix (Table A1).

$$\begin{aligned} Response = F_0 &+ F_i \times T + F_i \times C + F_i \times T \times C + F_i \times T^2 + F_i \times C^2 + F_i \times T^2 \times C \\ &+ F_i \times T \times C^2 + F_i \times T^3 + F_i \times C^3 + F_i \times T^2 \times C^2 + F_i \times T^3 \times C + F_i \\ &\times T \times C^3 + F_i \times T^4 + F_i \times C^4 \end{aligned} \tag{17}$$

where T = Temperature, C = Rh content, and F_i are "*Actual Factors*" listed in Table 3.

Table 3. Results of regression analysis and the Analysis of Variance (ANOVA) for the model of the experimental data for activity and yield of $RhPt/CeO_2$ catalysts evaluated in steam reforming of ethanol (SRE).

Variable*/Parameter	Ethanol Conversion (%)		H_2 Yield (mol H_2/mol EtOH Inlet)		CO Yield (mol CO/mol EtOH Inlet)	
	Coded Factors	Actual Factors	Coded Factors	Actual Factors	Coded Factors	Actual Factors
-	NS*	4.9×10^3	NS*	−34	NS*	32
T	NS*	−35	NS*	0.29	NS*	−0.22
C	-3.3×10^{10}	-2.2×10^3	2.1×10^9	−41	2.4×10^8	−21
T*C	3.9×10^7	11	NS*	0.1	NS*	0.1
T^2	1.5×10^5	9.1×10^{-2}	3.4×10^3	-8.8×10^{-4}	NS*	5.6×10^{-4}
C^2	-5.0×10^{10}	3.9×10^2	3.1×10^9	1.0×10^2	3.8×10^8	13
T^2*C	3.1×10^5	-1.8×10^{-2}	6.9×10^3	-1.2×10^{-4}	NS*	-1.7×10^{-4}
T*C^2	NS*	−3.8	NS*	-9.2×10^{-2}	NS*	-2.0×10^{-2}
T^3	1.5×10^3	-1.0×10^{-4}	NS*	1.1×10^{-6}	NS*	-6.0×10^{-7}
C^3	-3.6×10^9	1.6×10^3	2.1×10^9	-1.4×10^2	2.5×10^8	−14
T^2*C^2	1.5×10^5	2.8×10^{-3}	3.5×10^3	6.2×10^5	NS*	2.3×10^5
T^3*C	1.6×10^3	9.4×10^{-6}	NS*	-1.1×10^{-3}	NS*	9.1×10^{-8}
T*C^3	NS*	0.71	NS*	-5.2×10^{-10}	NS*	-4.7×10^{-3}
T^4	21	4.2×10^{-8}	NS*	85	NS*	2.4×10^{-10}
C^4	-8.5×10^9	-1.4×10^3	5.3×10^8	85	6.2×10^7	10
Model	Quartic		Quartic		Quartic	
F-value	164.08		480.03		200.86	
Probability F	$<1 \times 10^{-4}$		$<1 \times 10^{-4}$		$<1 \times 10^{-4}$	
Standard deviation	5.4		0.12		0.07	
Mean	72.0		1.53		0.55	
R^2	0.97		0.990		0.977	
Adjusted R^2	0.97		0.998		0.973	
Predicted R^2	0.96		0.984		0.964	
Adequate precision	37.09		81.95		57.84	
Lack of Fit	74		73		79	

Table 3. *Cont.*

Variable*/Parameter	CO_2 Yield (mol CO_2/mol EtOH Inlet)		CH_4 Yield (mol CH_4/mol EtOH Inlet)		Ethylene Yield (mol Ethylene/mol EtOH Inlet)	
	Coded Factors	Actual Factors	Coded Factors	Actual Factors	Coded Factors	Actual Factors
-	NS*	34	NS*	4.9	NS*	2.1
T	-6.0×10^5	-0.23	2.1×10^5	-3.5×10^{-2}	NS*	-1.5×10^{-2}
C	-3.4×10^8	2.1	-5.1×10^8	-0.52	NS*	-3.2×10^{-2}
T*C	-1.8×10^6	1.7×10^{-2}	6.4×10^5	2.9×10^{-4}	-5.9×10^{-2}	1.8×10^{-4}
T^2	-4.0×10^3	6.1×10^{-4}	NS*	8.9×10^5	NS*	3.9×10^5
C^2	-5.1×10^8	-57	-7.7×10^8	-6.0	0.14	-7.4×10^5
T^2*C	-8.1×10^3	-5.7×10^5	NS*	2.2×10^5	NS*	-2.8×10^{-7}
T*C^2	-1.8×10^6	0.13	6.4×10^5	-2.3×10^{-2}	NS*	-4.5×10^{-7}
T^3	NS*	-7.5×10^{-7}	NS*	-9.7×10^{-8}	NS*	-4.5×10^{-8}
C^3	-3.4×10^8	40	-5.2×10^8	27	NS*	3.3×10^{-6}
T^2*C^2	-4.0×10^3	-7.2×10^5	NS*	4.1×10^{-6}	NS*	1.2×10^{-10}
T^3*C	NS*	3.6×10^{-8}	NS*	-1.8×10^{-8}	NS*	1.6×10^{-10}
T*C^3	-6.1×10^5	-3.3×10^{-2}	2.2×10^5	1.2×10^{-2}	NS*	2.1×10^{-9}
T^4	NS*	3.5×10^{-10}	NS*	3.9×10^{-11}	NS*	1.9×10^{-11}
C^4	-8.6×10^7	-14	-1.3×10^8	-21	-0.14	-2.2×10^{-8}
Model	Quartic		Quartic	-	Quartic	-
F-value	42.55		47.39	-	3.2	-
Probability F	$<1 \times 10^{-4}$		$<1 \times 10^{-4}$	-	7×10^{-4}	-
Standard deviation	0.12		0.04	-	0.02	-
Mean	0.63		0.13	-	0.01	-
R^2	0.902		0.911	-	0.851	-
Adjusted R^2	0.880		0.892	-	0.828	-
Predicted R^2	0.812		0.864	-	0.820	-
Adequate precision	30.77		26.01	-	7.65	-
Lack of Fit	72		74	-	73	-

* Nonsignificant term.

The RSM analysis may give an indication of the relative effect of each variable on the response (activity or selectivity) [36]. According to the ANOVA (Table 3), RhPt/CeO_2 catalysts have a statistically significant effect on ethanol conversion. In addition, combined and individual contributions of both variables, temperature (T) and Rh content (C), were detected during SRE (Table 3). C, T^2, C^2, T^2C, T^3, C^3, T^2C^2, T^3C, T^4, and C^4 were significant terms in the ethanol conversion and H_2 yield models. Moreover, "*Coded Factors*" (Table 3) indicated the relative impact of the factors by comparing the factor coefficients [36]. Accordingly, C, C^2, C^3, and C^4 have higher relative impacts among these factors. Thus, although temperature influences SRE, Rh content (and thus Rh–Pt ratio) has a main role in ethanol conversion and the H_2 yield.

On the other hand, the ANOVA (Table 3) indicates that those terms related to the Rh content in the catalyst (C, C^2, C^3, and C^4) and some of its interactions with temperature (TC, T^2C, T^2C^2, and TC^3) are significant for yield models. The significant effect of the catalyst in SRE is due to the nature of the active site, which promotes different reaction mechanisms, as explained in Section 2.1. Thus, the possible formation of Rh–Pt alloys could explain the change in product distribution during SRE. Combining the mathematical models, $Rh_{0.4}Pt_{0.4}/CeO_2$ was selected as the best catalyst for SRE because of its combination of the highest H_2 yield, low ethylene formation, and smaller amount of CH_4 compared to the other bimetallic catalysts. However, it is important to determine the Rh–Pt effect on the overall energy integration of the system in order to select the best active metals ratio based on actual engineering application parameters. Therefore, the RSM models were integrated with Aspen Plus for the energy analysis of the Reformer–FC system.

2.3. Energy Analysis from RSM and Aspen Plus Integration

Power generation in FC fed with H_2 obtained from SRE is recognized as a promising energy model with high commercial value [64]. However, information about the energy efficiency of the process is still limited. Thus, RSM models were integrated with Aspen Plus to assess the energy production in an FC fed with H_2 from ethanol. Figure 2 shows the flowsheet of the simulation used. The process can be divided into three general stages: (i) H_2 production by SRE with preheating (HE1) to ensure the reaction temperature; (ii) H_2 purification by water condensation (CDS), CO elimination by carbon monoxide preferential oxidation (PROX) with preheating (HE2) to ensure the reaction temperature (150 °C [65]), and CH_4 and CO_2 adsorption (ADS) with activated carbon and precooling (HE3) to ensure the adsorption temperature (70 °C [66]); and (iii) energy generation in FC with preheating (HE4) to ensure the reaction temperature (150 °C [67]). The energy divisor (ED) indicates that the FC produces both electrical (40%) and heat (60%) energy [68]. CO_2 and CH_4 adsorption (ADS) with activated carbon was selected among other methods like adsorption with oxides [69,70], because the first ensures simultaneously removal of CO_2 and CH_4 in post-reforming streams, requires less power consumption, and minimizes H_2 losses [66]. ADS was considered as an isothermal and adiabatic process due to the low contents of the adsorbates in the streams, operating at 70 °C, 1 bar, and 100% efficiency, as reported by [66].

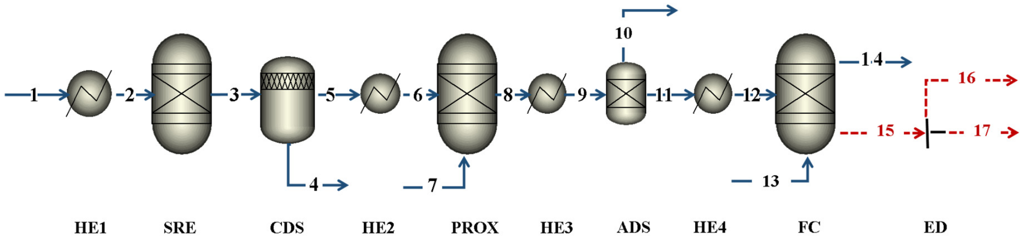

Figure 2. Aspen Plus flowsheet of the process used for the analysis of the energy production in FC fed with H_2 obtained through SRE of ethanol over Rh–Pt/CeO_2. Thermodynamic method = NRTL-SK. Equipment notation: HE—Heat exchanger, SRE—Reactor for the steam reforming of ethanol, CDS—Condenser, PROX—Reactor for carbon monoxide preferential oxidation, ADS—Adsorber, FC—Reactor as fuel cells, ED—Energy divisor. Streams notation: continuous lines are mass flows (1–14) and dashed lines are energy flows (15–17).

Figure 3 shows the error between the experimental data and the simulated data obtained from RSM-Aspen Plus integration for ethanol conversion (Figure 3a) and H_2 yield (Figure 3b) during SRE over Rh-Pt/CeO_2. Above 450 °C, an adequate prediction of the experimental data can be obtained with the RSM-Aspen Plus integration, with errors < 8% (Ln(*Error* (%)) = 2). At lower temperatures, the error was higher because the data was normalized assuming 100% carbon balance, which is not accurate at all the conditions. Actual carbon balances measured at each experiment were included Appendix (Table A1), where carbon balances lower than 100% can be ascribed to carbonaceous compounds and other products not quantified by gas chromatography (GC).

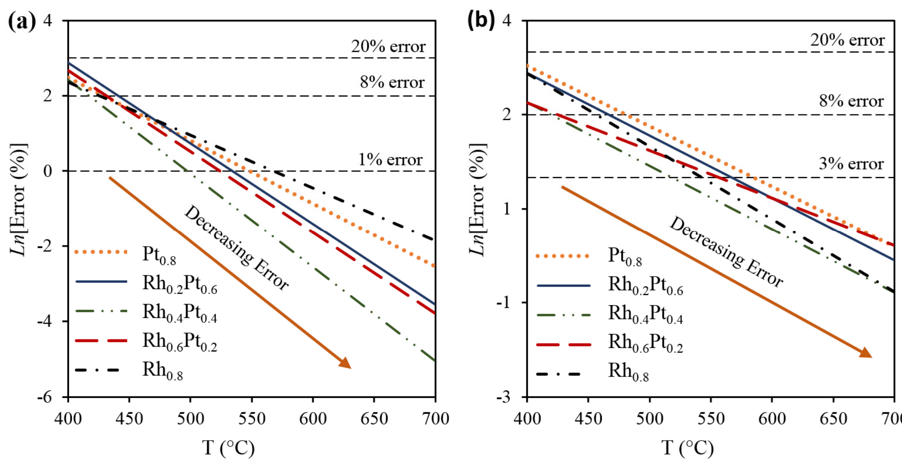

Figure 3. Percentage errors between the experimental data and the results from the RSM-Aspen Plus integration for (**a**) ethanol conversion and (**b**) H_2 yield during SRE over Rh–Pt/CeO_2. Note that the vertical axis was linearized using Ln to make the difference between the errors more visible.

In order to validate that the RSM-Aspen Plus integration can still accurately predict the experimental data, independent and random experiments outside the model were performed. Table 4 shows these results and their comparison to the simulated data. Experimental and predicted data are similar even for the catalysts evaluated at low temperature (430 and 470 °C), showing that the information obtained from RSM-Aspen Plus integration closely approximates the experimental results, and thus, it can be used to make predictions, as a preliminary energy analysis of SRE on $RhPt/CeO_2$ catalysts.

Table 4. Comparison between experimental data and values predicted by RSM-Aspen Plus integration.

Rh Content in Catalyst (wt %) [1]	*T* (°C)	Yield (mol/mol EtOH Inlet) [2]								Ethanol Conversion (%)	
		H_2		CO		CH_4		CO_2			
		E	*S*	*E*	*S*	*E*	*S*	*E*	*S*	*E*	*S*
0	430	1.0	1.2	0.0	0.0	0.0	0.0	0.8	0.8	36	33
0.2	630	2.1	2.0	0.7	0.9	0.6	0.4	0.1	0.6	96	100
0.4	530	1.0	0.9	0.5	0.5	0.2	0.2	0.7	0.7	71	72
0.6	470	0.2	0.3	0.4	0.2	0.2	0.2	0.3	0.7	66	61
0.8	610	2.1	2.1	1.4	1.3	0.1	0.1	0.4	0.4	96	97

[1] SRE over $RhPt/CeO_2$ with different Rh–Pt ratios. Total metal loading (Rh + Pt) = 0.8 wt % in all catalysts. Reaction conditions: $S/E = 3$, 100 mg catalyst, and $GHSV = 70{,}600\ h^{-1}$; [2] *E* = experimental data and *S* = values predicted by RSM-Aspen Plus integration.

Figure 4 shows the energy requirements calculated from the RSM-Aspen Plus integration in the SRE reactor as a function of the active metal content and temperature. Energy consumption per mole of ethanol inlet increased with temperature (Figure 4a). This is expected because ethanol reforming, an endothermic process (347 kJ/mol), is favored at higher temperatures [9]. At temperatures <500 °C, energy requirement decreased, likely due to the presence of an exothermic reaction, such as WGSR (−41.2 kJ/mol) [71]. Llera et al. [54] reported that the activation energy and changes in enthalpy are closely related to intermediate reactions occurring during SRE. Then, the difference in the energy requirements of each catalyst could be an indication that the Rh–Pt ratio favors different reaction mechanisms, as previously discussed in Section 2.1. The energy consumption per mole of H_2 produced (Figure 4b) indicates that the bimetallic Rh–Pt catalyst consumed slightly more energy at high temperatures (>500 °C). The $Rh_{0.4}Pt_{0.4}$ catalyst promotes greater energy consumption at 700 °C. This catalyst also showed a higher H_2 yield (Figure 1b) with total ethanol conversion (Figure 1a), little CH_4 formation (Figure 1d), and ethylene (Figure 1f) formation. The reforming of ethanol (Equation (1)), CH_4 (Equation (8)), and ethylene (Equation (10)) to produce H_2 are endothermic reactions [24]. Thus, the increased production of H_2 on $Rh_{0.4}Pt_{0.4}/CeO_2$ could be attributed to the fact that this catalyst promotes further endothermic reactions, which require greater energy consumption. Conversely, $Rh_{0.6}Pt_{0.2}/CeO_2$ showed lower energy consumption at temperatures below 500 °C (Figure 4b). At these temperatures, $Rh_{0.6}Pt_{0.2}/CeO_2$ also showed low conversion of ethanol (Figure 1a), limited H_2 (Figure 1b) and CO yields (Figure 1c), and higher CH_4 (Figure 1d) and ethylene (Figure 1f) yields, which can be an indication that exothermic reactions, such as WGSR (Equation (2)) and reversible reforming, are taking place. Rabenstein et al. [9] reported that greater energy demands are needed to maximize H_2 production because the H_2 yield is favored by endothermic reactions. Accordingly, the Rh–Pt ratio that favored an increase in H_2 production required a slight increase in the energy demand.

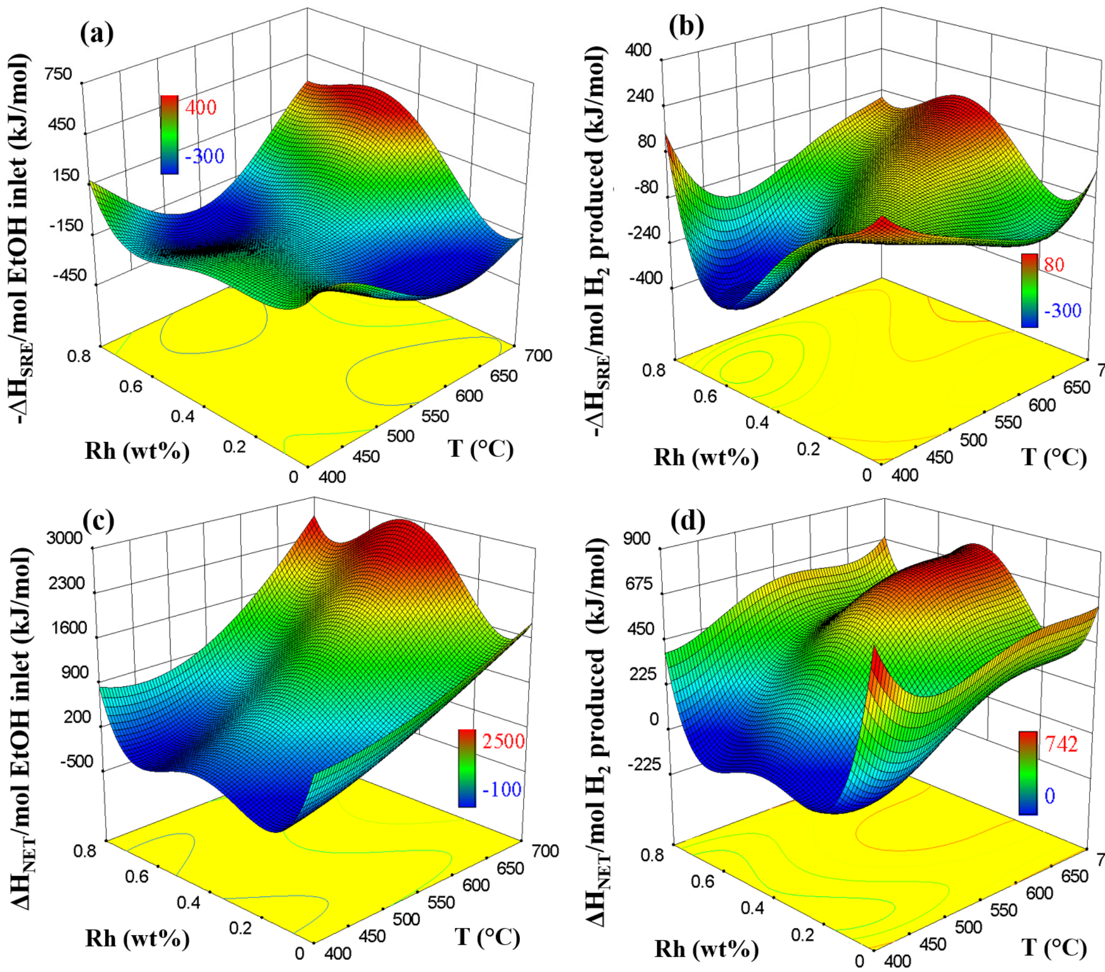

Figure 4. Changes in enthalpy during the SRE and net energy production of the system computed with Aspen Plus in terms of ethanol-inlet ((**a**) and (**c**)) and H_2 ((**b**) and (**d**)) produced. Total metal loading (Rh + Pt) = 0.8 wt % in all Rh–Pt/CeO_2 catalysts. Response surface: Quartic model, $R^2 > 0.85$; Adjusted, $R^2 > 0.8$, *Probability F* << 0.1 (significant) and *Lack of Fit* >> 3 (nonsignificant).

The net energy produced in the system was obtained according to Equation (18), where ΔH_{NET} is the net available energy of the system, ΔH_{FC} is the change in enthalpies in the FC, ΔH_{HE4} is the change in enthalpies in the heating of the stream entering the FC, ΔH_{PROX} is the change in enthalpies during the PROX, ΔH_{HE2} is the change in enthalpies in the heating of the stream entering the PROX, ΔH_{CDS} is the change in enthalpies in the condenser, ΔH_{SRE} is the change in enthalpies during the SRE, ΔH_{HE1} is the change in enthalpies during the initial heat exchange, and ΔH_{HE3} is the change in enthalpies in the cooling of the stream entering the ADS. CH_4 and CO_2 separator (ADS) was not taken into account in the energy analysis because it was considered as an non-reactant, isothermal, and adiabatic process $\Delta H = 0$, which operates at 70 °C and 1 bar [66]. However, the precooling (HE3) to ensure the operating temperature in ADS was included.

$$\Delta H_{NET} = \Delta H_{FC} + \Delta H_{HE4} + \Delta H_{PROX} + \Delta H_{HE2} + \Delta H_{CDS} + \Delta H_{SRE} + \Delta H_{HE1} + \Delta H_{HE3} \quad (18)$$

The net energy (ΔH_{NET}) production obtained per mol of ethanol inlet is shown in Figure 4c. The process is feasible ($\Delta H_{NET} > 0$) at temperatures > 480 °C, where the H_2 yield is $\geq$ 1.2 mol H_2/mol EtOH inlet (Figure 1b). At low temperatures (<500 °C) on bimetallic $Rh_{0.2}Pt_{0.6}/CeO_2$ and $Rh_{0.6}Pt_{0.2}/CeO_2$ catalysts, the energy obtained by feeding the FC with H_2 is not enough to compensate for the energy required to heat the feed stream, conduct the SRE, and purify the H_2. $Rh_{0.4}Pt_{0.4}/CeO_2$

showed the best energy performance, reaching a minimum at 400 °C (39 kJ/mol EtOH inlet) and a maximum at 700 °C (3149 kJ/mol EtOH inlet) of net energy production. Freni et al. [72] studied a system based on a molten carbonate fuel cell fed directly with a solution of ethanol (S/E = 3), operating at greater than 600 °C. The authors reported that it is possible to obtain up to 1318 kJ/mol EtOH inlet. The major limitation of this system is the generation of byproducts such as CO, which affect the performance of the FC. The results reported in this paper confirm that it is energetically feasible to carry out H_2 production and purification in separated steps in order to ensure good quality of the H_2 streams that are fed into the FC, but avoiding a low temperature WGSR reactor.

Figure 4d shows the net energy production per mol of H_2 obtained in SRE. Pt/CeO_2 showed a net energy production of 674 kJ/mol H_2 produced at low temperatures (<450 °C) due to the energy requirements to heat the feed stream in the first heat exchanger (HE1, Figure 2) are low (<2700 kJ/mol EtOH) and exothermic reactions are taking place at these temperatures in the SRE reactor ($-\Delta H_{SRE}$ < 130 kJ/mol EtOH). Moreover, H_2 production on this catalyst was 0.7 mol H_2/mol EtOH (Figure 1b), which increased the value of the ΔH_{NET}/mol H_2 produced ratio. However, only 491 kJ/mol EtOH inlet was delivered using this Pt/CeO_2 catalyst at temperatures <450 °C, which is considerably lower when compared to other catalysts at >550 °C (>812 kJ/mol EtOH inlet, Figure 4c). In this way, energy production must be jointly analyzed by H_2 produced and ethanol inlet, to avoid mistaken interpretations.

Therefore, although a higher requirement of energy is needed to produce more H_2 (Figure 4b), the overall energy efficiency increases significantly with additional produced H_2. Accordingly, it is desirable to produce a high amount of H_2 despite the additional energy requirements. At 700 °C, $Rh_{0.4}Pt_{0.4}/CeO_2$ showed a maximum in net energy (742 kJ/mol H_2 produced). Until now, only 40% of this energy could be transformed into electricity in FC [68]; this corresponds to 297 kJ/mol H_2 produced, which is in line with previous reports. Lopes et al. [64] evaluated a system based on ethanol reforming and a 5 kW proton exchange membrane fuel cell (PEMFC), reporting that the net energy production of the system was around of 286 kJ/mol H_2 produced. Sanchez et al. [73] conducted an energy analysis of the production of electricity in FC fed with H_2 from the steam reforming of bioethanol, reporting a net energy production of 156 kJ/mol H_2 produced. Those calculations included glucose fermentation and bioethanol purification steps.

Consequently, the RhPt/CeO_2 catalyst with a Rh–Pt ratio of 1:1 is a promising catalyst for SRE because it promotes higher H_2 yields with low formation of undesirable byproducts, such as CH_4 and ethylene. Furthermore, it could be energetically sustainable to include this catalyst in a system for energy production in FC fed with H_2 obtained from SRE.

3. Materials and Methods

3.1. Catalyst Synthesis

RhPt/CeO_2 catalyst samples with different Rh–Pt weight ratios (Table 2) were prepared by the incipient wetness co-impregnation method according to previous reports [32,37]. This method was selected because is effective to load active metals in metal oxide supports and ensure high dispersion [34,74]. A total metal loading of 0.8 wt % was kept in all the catalysts in order to reduce sintering [34]. Cerium nitrate hexahydrate ($Ce(NO_3)_2 \cdot 6H_2O$, 99.5%, Alfa Aesar, Haverhill, MA, USA) was calcined at 700 °C in a muffle for 2 h to obtain CeO_2, which was used as support. Then, the active metal were co-impregnated by mixing the needed amount of rhodium(III) chloride hydrate ($RhCl_3 \cdot H_2O$, Sigma Aldrich Chem. Co., St. Louis, MO, USA) and hexachloroplatinum acid hexahydrate ($H_2PtCl_6 \cdot 6H_2O$, Aldrich Chem. Co.) solutions in water, and slowly added onto the support. The metal–support mixture was stirred, dried at 105 °C for 24 h, and calcined at 700 °C in muffle for 2 h.

3.2. Catalytic Tests

RhPt/CeO_2 catalysts were evaluated in a fixed bed reactor (internal diameter = 12 mm) at atmospheric pressure under kinetic control, according to a previous report [37]. For that, a liquid mixture with a stoichiometric molar ratio of ethanol to water S/E = 3 (0.03 mL/min) was pumped into an evaporator (200 °C, atmospheric pressure) using a Simdos 02 metering pump (KNF Neuberger, Trenton, NJ, USA) and then mixed with N_2 carrier gas (300 mL/min). This mixture was fed into the reactor, which was placed in an electric furnace (Applied Test Systems, Butler, PA, USA) with temperature control. RhPt/CeO_2 catalysts (100 mg) were diluted with inert quartz particles (80-mesh) until completion of a 300 mg total catalytic bed. To diminish external and internal mass transfer limitations, the plug flow reactor condition was achieved through the elimination of back mixing and channeling by maintaining the ratio of the catalyst bed height and catalyst particle size (L/D_p) at 50 and the ratio of the reactor internal diameter and catalyst particle size (D/D_p) at 60 [3,75]. Before the reaction, the catalysts were reduced in situ in 10% H_2/N_2 (300 mL/min) at 700 °C for 1 h. Catalytic activity tests were started at 700 °C and the temperature was decreased in 20 °C intervals to 400 °C (continuous sequence, 25 min at each temperature). A gaseous space velocity (*GHSV*) of 70,600 h^{-1} with a molar composition inlet of the reformer of ethanol (0.018), water (0.054), and N_2 (0.928) was fixed.

Post-reforming stream (N_2, H_2, CH_4, CO, CO_2, ethanol, and ethylene) was quantified by gas chromatography using a Clarus 580 equipment (GC, Perkin Elmer, Waltham, MA, USA) equipped with a Carboxen 1010 plot column (30 m, 0.53 mm ID, Restek, Bellefonte, PA, USA) and a Innowax column (30 m, 0.53 mm ID, Perkin Elmer, USA) connected to a thermal conductivity detector (TCD) and flame ionization detector (FID), respectively. The ethanol conversion (X_{EtOH}) and yield for each detected product were calculated according to Equations (19) and (20), where $F_{\text{EtOH,inlet}}$ is the initial theoretical mole flow (mol/min) of ethanol at standard conditions, $F_{\text{EtOH,outlet}}$ is the mole flow (mol/min) of unreacted ethanol in the product stream detected by GC at time t, and F_i is the mole flow (mol/min) of product i (H_2, CO, CH_4, CO_2, C_2H_4 or C_2H_6). Carbon balance for each experiment was included as Appendix (Table A1).

$$X_{\text{EtOH}} = \frac{F_{\text{EtOH,inlet}} - F_{\text{EtOH,outlet}}}{F_{\text{EtOH,inlet}}} \tag{19}$$

$$Yield_i = \frac{F_i}{F_{\text{EtOH,inlet}}} \tag{20}$$

All catalysts samples were characterized by thermalgravimetric analysis (TGA) to identify possible carbonaceous residues on the catalyst surface. The TGA analysis was performed in a thermogravimetric analyzer (Mettler Toledo, Columbus, OH, USA). Each sample (30 mg) was degassed with 30 mL/min of N_2 flowing at 100 °C for 1 h and heated to 1000 °C in air (5 °C/min, 200 mL/min).

3.3. Statistical Analysis

Experiments completely randomized with five treatments and three replications were conducted. Catalytic performance of RhPt/CeO_2 catalysts was evaluated by response surfaces using Design Expert 8 software (version 8.0, Stat-Ease, Inc., Minneapolis, MN, USA, 2009). The adjustment of the response surfaces was validated by the probability ("*Probability F*"), "*Lack of fit*" test, "*Adequate precision*", and variability with respect to the experimental data (R^2). "*Probability F*" is used to refuse the null hypothesis that all coefficients are 0 and it was computed from "*F-value*", which is the mean square model divided into the mean square residual [76]. "*Lack of fit*" is a statistical test to indicate if the model fits well. "*Probability F*" and "*Lack of fit*" can be used as criteria to select adequate model [63] because they are related to the significance of the terms. Similarly, "*Adequate precision*" is a signal to noise ratio present in the model. R^2 values close to 1.0 and "*Probability F* " less than 0.5 are expected in a significant model [36]. Also, a minimum of 3 for "*Lack of fit*" (nonsignificant) and 4 for "*Adequate precision*" are recommended by Design Expert 8 software [63]. Favorable operation zones in SRE for high production of H_2 were identified.

3.4. Simulation in Aspen Plus Software

The mathematical models obtained from RSM were used to make energy predictions in Aspen Plus. Figure 2 shows the simulation flowsheet. First, experimental data were normalized in Microsoft Excel 2016 (Microsoft, Silicon Valley, CA, USA) until complete 100% carbon balance. Thus, the block named "SRE" was used to link Aspen Plus V9.0 (Aspen Tech, Burlington, MA, USA, 2016) and Microsoft Excel 2016. NRTL-RK was used as thermodynamic package in the simulations in order to simultaneously model condensable and non-condensable compounds present in hydrocarbon reforming [39,77]. This allowed the results of the simulations to be downloaded directly into Excel and used in the mathematical models obtained from the RSM, replacing the "*Actual Factors*" of Table 3 in Equation (17). The percentage error between the experimental data and the results of the RSM and Aspen Plus integration was calculated according to Equation (21), where Error is the relative error, D_{exp} is the experimental data, and D_{simu} is the result obtained by RSM-Aspen Plus integration. This error was plotted in Figure 3 as natural logarithmic ordinate (Ln(*Error* (%))). In addition, independent and random catalytic tests outside the statistical model were performed as an additional confirmation and included in Table 4.

$$Error = \frac{|D_{\text{Exp}} - D_{\text{Simu}}|}{D_{\text{Exp}}} \times 100 \quad (21)$$

According to Figure 2, a heat exchanger (HE1) was previously used to heat the feed from 20 °C to the reaction temperature. A condenser (CDS) at 40 °C was used to completely remove water. A yield reactor (PROX) was used to remove CO from the H_2 stream, assuming a total CO conversion, and preheating (HE2) ensured the reaction temperature (150 °C) [65]. Then, a total separator (ADS) with precooling (HE3) was used to completely remove CH_4 and CO_2 assuming isothermal and adiabatic adsorption, due to their low concentration in the stream. ADS simulates an adsorber filled with activated carbon that operates at 70 °C, 1 bar, and 100% efficiency [66]. Finally, the FC was modeled as a reactor (FC) operating at 150 °C [67], with a preheating (HE4) to ensure this condition, and 80% H_2 conversion and 40% electrical efficiency were assumed in FC [68]. Aspen Plus was used to calculate the enthalpies of each stream in order to determine the energy requirements in each equipment of the system (Figure 2) per mole of ethanol inlet and per mol of H_2 produced in SRE according to Equations (22) and (23), respectively, where ΔH_i is the total change of enthalpy in the equipment i (i.e., HE1, SRE, CDS, PROX, HE2, HE3, HE4, or FC); H_{S1i} and H_{S2i} are the total enthalpy (kJ/min) in the inflow and outflow of equipment i, respectively; $F_{\text{H2,outlet}}$ is the mole flow (mol/min) of H_2 produced in the SRE; and $F_{\text{EtOH,inlet}}$ is the initial theoretical mole flow (mol/min) of ethanol at ambient temperature. Sensitivity analyses for temperature (400–700 °C) and different Rh–Pt ratios in the catalyst were performed in order to build a surface response in Design Expert 8 software. The net energy produced in the system was obtained according to Equation (18): it is expected that ΔH_{CDS}, ΔH_{PROX}, $\Delta H_{\text{HE3,}}$ and ΔH_{FC} are positive due to an energy release; that ΔH_{HE1}, ΔH_{HE2}, and ΔH_{HE4} are negative because of energy consumption; and that ΔH_{SRE} can be positive or negative depending on the operating temperature.

$$\Delta H_i = \frac{\sum H_{S1i} - \sum H_{S2i}}{F_{\text{EtOH,intlet}}} \quad (22)$$

$$\Delta H_i = \frac{\sum H_{S1i} - \sum H_{S2i}}{F_{\text{H}_2\text{,outlet}}} \quad (23)$$

4. Conclusions

The integration of the Response Surface Methodology (RSM) and Aspen Plus enabled the assessment of energy generation in a fuel cell (FC). FC was fed with H_2 obtained from the steam reforming of ethanol (SRE) over RhPt/CeO_2 catalysts. The effect of the operating temperature and the Rh–Pt weight ratio (1:0, 3:1, 1:1, 1:3, and 0:1) on SRE over RhPt/CeO_2 was evaluated using RSM. A maximum of 4.2 mol H_2/mol EtOH (700 °C) with the $Rh_{0.4}Pt_{0.4}/CeO_2$ catalyst was obtained. The mathematical models obtained from the RSM were integrated into Aspen Plus through Excel in order to simulate an integrated H_2 production by SRE; H_2 purification by water condensation, preferential oxidation of CO, and a CH_4 and CO_2 adsorber; and energy generation in an FC. An energy sensitivity analysis of the process carried out in Aspen Plus was employed to generate new response surfaces. The response surfaces showed that an increase in H_2 production requires more energy consumption in SRE. However, the higher the H_2 production, the higher is the energy generation in the FC, which increased the overall system efficiency. A yield of 1.2 mol H_2/mol EtOH was identified as the minimum necessary to make the system energetically feasible. A maximum net energy of 742 kJ/mol H_2 was produced at 700 °C when using a $Rh_{0.4}Pt_{0.4}/CeO_2$ catalyst for SRE. The portion of this energy that could be transformed into electricity in FC was 40% (297 kJ/mol H_2 produced). According to the results of the integration of RSM and Aspen Plus, $Rh_{0.4}Pt_{0.4}/CeO_2$ is a promising catalyst for use in an energy production system that uses fuel cells fed with H_2 obtained from ethanol.

Acknowledgments: The authors are grateful to Colciencias and Universidad de La Sabana for the financial support of this work through the project number ING-163 (Colciencias contract 174-2016).

Author Contributions: Bernay Cifuentes and Martha Cobo contributed equally to this work. Manuel Figueredo participated in the integration of the mathematical models from Response Surface Methodology (RSM) with Aspen Plus. All authors contributed to the writing and review of this document.

Conflicts of Interest: This manuscript has not been published or presented elsewhere in part or entirety, and it is not under consideration by another journal. All the authors have approved the manuscript and agreed to its submission to your esteemed journal. There are no conflicts of interest to declare.

Appendix

Table A1. Experimental results used to obtain response surfaces and carbon balances.

Rh Content (wt %)	T (°C)	Carbon Balance (%)	Yield (mol/mol EtOH Inlet)					Ethanol Conversion (%)
			H_2	CO	CH_4	CO_2	Ethylene	
0.0	700	93	3.11	1.09	0.13	0.64	3.0×10^{-6}	100
0.0	680	96	2.84	0.92	0.16	0.85	2.9×10^{5}	100
0.0	660	91	2.52	0.98	0.19	0.65	5.0×10^{5}	100
0.0	640	94	2.19	0.72	0.32	0.84	2.4×10^{-4}	100
0.0	620	92	1.96	0.82	0.18	0.83	1.1×10^{5}	99.3
0.0	600	92	1.66	0.78	0.01	0.85	2.4×10^{-4}	90.5
0.0	580	97	1.60	0.65	0.03	0.91	1.6×10^{-4}	82.8
0.0	560	99	1.28	0.36	0.08	1.08	4.5×10^{-4}	76.9
0.0	540	95	1.26	0.30	0.06	0.96	3.3×10^{5}	71.1
0.0	520	96	1.19	0.10	0.09	1.09	5.0×10^{5}	68.1
0.0	500	107	1.11	0.09	0.02	1.02	9.7×10^{5}	49.7
0.0	480	109	1.13	0.07	0.04	0.82	3.5×10^{-4}	36.8
0.0	460	109	1.13	0.12	0.00	0.82	5.3×10^{-4}	37.7
0.0	440	106	1.15	0.01	0.00	0.81	3.7×10^{5}	35.5
0.0	420	107	1.15	0.00	0.00	0.73	4.0×10^{-4}	29.8
0.0	400	108	0.96	0.00	0.00	0.81	6.6×10^{-3}	33.7
0.2	700	97	3.15	0.97	0.31	0.65	2.1×10^{-4}	100
0.2	680	93	2.87	0.78	0.44	0.63	1.1×10^{-4}	100
0.2	660	92	2.54	0.84	0.46	0.55	2.9×10^{-4}	100
0.2	640	92	2.28	0.84	0.38	0.63	2.1×10^{-4}	100
0.2	620	95	1.80	0.86	0.45	0.60	2.2×10^{-4}	100
0.2	600	89	1.49	0.80	0.35	0.61	0	99.1
0.2	580	94	1.29	0.74	0.27	0.82	7.7×10^{5}	97.4

Table A1. *Cont.*

Rh Content (wt %)	*T* (°C)	Carbon Balance (%)	Yield (mol/mol EtOH Inlet)					Ethanol Conversion (%)
			H_2	CO	CH_4	CO_2	Ethylene	
0.2	560	89	1.18	0.39	0.43	0.59	0	81.6
0.2	540	93	1.02	0.32	0.25	0.60	1.0×10^{-4}	65.4
0.2	520	91	0.53	0.13	0.24	0.59	1.3×10^{-4}	57.0
0.2	500	96	0.46	0.10	0.15	0.71	1.5×10^{-4}	51.8
0.2	480	104	0.35	0.06	0.06	0.89	7.0×10^{-4}	46.6
0.2	460	110	0.31	0.02	0.04	1.02	1.3×10^{-3}	44.0
0.2	440	102	0.15	0.01	0.05	0.51	2.3×10^{-3}	26.6
0.2	420	105	0.18	0.01	0.04	0.80	1.9×10^{-3}	37.7
0.2	400	108	0.10	0.01	0.02	0.90	7.2×10^{5}	39.0
0.4	700	96	4.10	1.34	0.26	0.31	7.7×10^{5}	100
0.4	680	100	3.81	1.25	0.25	0.50	6.0×10^{5}	100
0.4	660	96	3.32	1.24	0.26	0.42	8.2×10^{5}	100
0.4	640	90	2.90	0.89	0.41	0.50	1.0×10^{-4}	100
0.4	620	91	2.68	0.98	0.50	0.34	0	100
0.4	600	79	2.38	0.95	0.18	0.43	4.5×10^{-3}	100
0.4	580	93	2.08	0.94	0.17	0.75	4.5×10^{-3}	100
0.4	560	92	1.54	0.65	0.30	0.59	1.2×10^{-2}	85,8
0.4	540	96	0.91	0.50	0.21	0.68	1.2×10^{-2}	75.3
0.4	520	93	0.90	0.47	0.09	0.65	1.2×10^{-2}	68.5
0.4	500	103	0.81	0.22	0.07	0.69	1.2×10^{-2}	47.4
0.4	480	108	0.65	0.10	0.11	0.75	1.1×10^{-2}	41.6
0.4	460	104	0.48	0.01	0.00	0.69	2.1×10^{-3}	31.0
0.4	440	107	0.37	0.01	0.00	0.75	2.2×10^{-4}	31.3
0.4	420	110	0.34	0.02	0.00	0.66	1.1×10^{-4}	23.5
0.4	400	109	0.32	0.02	0.00	0.66	2.2×10^{-7}	24.4
0.6	700	90	4.12	1.48	0.19	0.13	5.6×10^{-6}	100
0.6	680	100	3.40	1.28	0.22	0.50	2.4×10^{-4}	100
0.6	660	93	3.02	1.28	0.32	0.27	4.9×10^{-4}	100
0.6	640	93	2.41	0.96	0.28	0.61	4.8×10^{-4}	99.7
0.6	620	93	1.96	0.85	0.35	0.66	1.0×10^{-3}	100
0.6	600	92	1.67	0.94	0.29	0.61	5.2×10^{-4}	99.5
0.6	580	91	1.49	0.84	0.26	0.71	4.3×10^{-4}	99.4
0.6	560	94	1.24	0.83	0.43	0.62	8.6×10^{5}	100
0.6	540	100	0.95	0.74	0.27	0.73	0.13	100
0.6	520	93	0.72	0.69	0.17	0.75	7.7×10^{-2}	94.9
0.6	500	94	0.43	0.51	0.20	0.90	7.8×10^{-3}	87.4
0.6	480	107	0.20	0.19	0.19	0.89	0.13	70.1
0.6	460	101	0.18	0.18	0.12	0.59	7.7×10^{-2}	52.0
0.6	440	92	0.13	0.12	0.13	0.44	7.8×10^{-3}	44.0
0.6	420	93	0.09	0.09	0.00	0.37	3.8×10^{-2}	33.7
0.6	400	90	0.03	0.03	0.04	0.29	1.2×10^{-2}	29.1
0.8	700	98	4.07	1.71	0.04	0.19	4.5×10^{-3}	100
0.8	680	95	3.93	1.65	0.05	0.19	2.4×10^{5}	100
0.8	660	95	3.34	1.57	0.07	0.25	3.7×10^{-4}	99.8
0.8	640	91	2.65	1.42	0.08	0.33	4.8×10^{-4}	99.6
0.8	620	89	2.23	1.25	0.09	0.43	3.1×10^{-4}	99.2
0.8	600	97	1.89	1.31	0.09	0.41	1.1×10^{5}	93.7
0.8	580	89	1.39	0.85	0.11	0.61	1.8×10^{-3}	89.3
0.8	560	100	1.08	0.80	0.16	0.62	3.5×10^{-3}	79.2
0.8	540	104	1.10	0.72	0.08	0.76	4.2×10^{-3}	74.5
0.8	520	97	0.96	0.61	0.09	0.62	3.9×10^{-3}	69.5
0.8	500	91	0.95	0.58	0.01	0.46	2.1×10^{-3}	62.0
0.8	480	92	0.83	0.51	0.01	0.36	1.2×10^{-3}	51.8
0.8	460	89	0.67	0.37	0.00	0.30	2.6×10^{-3}	45.4
0.8	440	95	0.65	0.34	0.00	0.26	7.5×10^{-4}	35.1
0.8	420	99	0.67	0.31	0.00	0.29	1.2×10^{-3}	31.5
0.8	400	96	0.62	0.30	0.00	0.18	4.7×10^{-4}	28.3
Mean		97	-	-	-	-	-	-
Standard deviation		6.5	-	-	-	-	-	-

References

1. Rhodes, C.J. The 2015 Paris climate change conference: Cop21. *Sci. Prog.* **2016**, *99*, 97–104. [CrossRef] [PubMed]
2. Lucia, U. Overview on fuel cells. *Renew. Sustain. Energy Rev.* **2014**, *30*, 164–169. [CrossRef]
3. Sahoo, D.R.; Vajpai, S.; Patel, S.; Pant, K.K. Kinetic modeling of steam reforming of ethanol for the production of hydrogen over Co/Al_2O_3 catalyst. *Chem. Eng. J.* **2007**, *125*, 139–147. [CrossRef]

4. Quintero, J.A.; Montoya, M.I.; Sánchez, O.J.; Giraldo, O.H.; Cardona, C.A. Fuel ethanol production from sugarcane and corn: Comparative analysis for a Colombian case. *Energy* **2008**, *33*, 385–399. [CrossRef]
5. Elfasakhany, A. Investigations on the effects of ethanol–methanol–gasoline blends in a spark-ignition engine: Performance and emissions analysis. *Eng. Sci. Technol. Int. J.* **2015**, *18*, 713–719. [CrossRef]
6. Chiu, W.-C.; Horng, R.-F.; Chou, H.-M. Hydrogen production from an ethanol reformer with energy saving approaches over various catalysts. *Int. J. Hydrogen Energy* **2013**, *38*, 2760–2769. [CrossRef]
7. De Lima, S.; Da Cruz, I.; Jacobs, G.; Davis, B.; Mattos, L.; Noronha, F.B. Steam reforming, partial oxidation, and oxidative steam reforming of ethanol over Pt/$CeZrO_2$ catalyst. *J. Catal.* **2008**, *257*, 356–368. [CrossRef]
8. López, E.; Divins, N.J.; Anzola, A.; Schbib, S.; Borio, D.; Llorca, J. Ethanol steam reforming for hydrogen generation over structured catalysts. *Int. J. Hydrogen Energy* **2013**, *38*, 4418–4428. [CrossRef]
9. Rabenstein, G.; Hacker, V. Hydrogen for fuel cells from ethanol by steam-reforming, partial-oxidation and combined auto-thermal reforming: A thermodynamic analysis. *J. Power Sources* **2008**, *185*, 1293–1304. [CrossRef]
10. Liberatori, J.W.C.; Ribeiro, R.U.; Zanchet, D.; Noronha, F.B.; Bueno, J.M.C. Steam reforming of ethanol on supported nickel catalysts. *Appl. Catal. A* **2007**, *327*, 197–204. [CrossRef]
11. Valle, B.; Aramburu, B.; Remiro, A.; Bilbao, J.; Gayubo, A.G. Effect of calcination/reduction conditions of Ni/La_2O_3–αAl_2O_3 catalyst on its activity and stability for hydrogen production by steam reforming of raw bio-oil/ethanol. *Appl. Catal. B* **2014**, *147*, 402–410. [CrossRef]
12. Wang, H.; Zhang, L.; Yuan, M.; Xu, T.; Liu, Y. Steam reforming of ethanol over Ni/$Ce_{0.7}Pr_{0.3}O_2$ catalyst. *J. Rare Earths* **2012**, *30*, 670–675. [CrossRef]
13. Bilala, M.; Jackson, S.D. Ethanol steam reforming over Rh and Pt catalysts: Effect of temperature and catalyst deactivation. *Catal. Sci. Technol* **2013**, *3*, 754–766. [CrossRef]
14. Guerrero, L.; Castilla, S.; Cobo, M. Advances in ethanol reforming for the production of hydrogen. *Quim. Nova* **2014**, *37*, 850–856. [CrossRef]
15. Konsolakis, M.; Ioakimidis, Z.; Kraia, T.; Marnellos, G. Hydrogen production by ethanol steam reforming (ESR) over CeO_2 supported transition metal (Fe, Co, Ni, Cu) catalysts: Insight into the structure-activity relationship. *Catalysts* **2016**, *6*, 39. [CrossRef]
16. Liu, Y.; Murata, K.; Inaba, M. Steam reforming of bio-ethanol to produce hydrogen over Co/CeO_2 catalysts derived from $Ce_{1-x}Co_xO_{2-y}$ precursors. *Catalysts* **2016**, *6*, 26. [CrossRef]
17. Domínguez, M.; Taboada, E.; Molins, E.; Llorca, J. Co-Fe-Si aerogel catalytic honeycombs for low temperature ethanol steam reforming. *Catalysts* **2012**, *2*, 386–399. [CrossRef]
18. Sheng, P.Y.; Chiu, W.W.; Yee, A.; Morrison, S.J.; Idriss, H. Hydrogen production from ethanol over bimetallic Rh-M/CeO_2 (M = Pd or Pt). *Catal. Today* **2007**, *129*, 313–321. [CrossRef]
19. Sheng, P.-Y.; Yee, A.; Bowmaker, G.A.; Idriss, H. H_2 production from ethanol over Rh–Pt/CeO_2 catalysts: The role of Rh for the efficient dissociation of the carbon–carbon bond. *J. Catal.* **2002**, *208*, 393–403. [CrossRef]
20. Jacobs, G.; Keogh, R.A.; Davis, B.H. Steam reforming of ethanol over Pt/ceria with co-fed hydrogen. *J. Catal.* **2007**, *245*, 326–337. [CrossRef]
21. Zou, J.; Yu, B.; Zhang, S.; Zhang, J.; Chen, Y.; Cui, L.; Xu, T.; Cai, W. Hydrogen production from ethanol over Ir/CeO_2 catalyst: Effect of the calcination temperature. *Fuel* **2015**, *159*, 741–750. [CrossRef]
22. Calles, J.; Carrero, A.; Vizcaíno, A.; Lindo, M. Effect of Ce and Zr addition to Ni/SiO_2 catalysts for hydrogen production through ethanol steam reforming. *Catalysts* **2015**, *5*, 58–76. [CrossRef]
23. Gutierrez, A.; Karinen, R.; Airaksinen, S.; Kaila, R.; Krause, A.O.I. Autothermal reforming of ethanol on noble metal catalysts. *Int. J. Hydrogen Energy* **2011**, *36*, 8967–8977. [CrossRef]
24. Contreras, J.L.; Salmones, J.; Colín-Luna, J.A.; Nuño, L.; Quintana, B.; Córdova, I.; Zeifert, B.; Tapia, C.; Fuentes, G.A. Catalysts for H_2 production using the ethanol steam reforming (a review). *Int. J. Hydrogen Energy* **2014**, *39*, 18835–18853. [CrossRef]
25. Moura, J.S.; Souza, M.O.G.; Bellido, J.D.A.; Assaf, E.M.; Opportus, M.; Reyes, P.; do Carmo Rangel, M. Ethanol steam reforming over rhodium and cobalt-based catalysts: Effect of the support. *Int. J. Hydrogen Energy* **2012**, *37*, 3213–3224. [CrossRef]
26. Cobo, M.; Pieruccini, D.; Abello, R.; Ariza, L.; Córdoba, L.F.; Conesa, J.A. Steam reforming of ethanol over bimetallic RhPt/La_2O_3: Long-term stability under favorable reaction conditions. *Int. J. Hydrogen Energy* **2013**, *38*, 5580–5593. [CrossRef]
27. Ratnasamy, C.; Wagner, J.P. Water gas shift catalysis. *Catal. Rev.* **2009**, *51*, 325–440. [CrossRef]

28. Mei, Z.; Li, Y.; Fan, M.; Zhao, L.; Zhao, J. Effect of the interactions between Pt species and ceria on Pt/ceria catalysts for water gas shift: The XPS studies. *Chem. Eng. J.* **2015**, *259*, 293–302. [CrossRef]
29. Holgado, J.P.; Munuera, G. XPS/TPR study of the reducibility of M/CeO_2 catalysts (M = Pt, Rh): Does junction effect theory apply? *Stud. Surf. Sci. Catal.* **1995**, *96*, 109–122.
30. Ni, M.; Leung, D.Y.C.; Leung, M.K.H. A review on reforming bio-ethanol for hydrogen production. *Int. J. Hydrogen Energy* **2007**, *32*, 3238–3247. [CrossRef]
31. O'Brien, F.J. Biomaterials & scaffolds for tissue engineering. *Mater. Today* **2011**, *14*, 88–95.
32. Cifuentes, B.; Valero, M.F.; Conesa, J.A.; Cobo, M. Hydrogen production by steam reforming of ethanol on Rh-Pt catalysts: Influence of CeO_2, ZrO_2, and La_2O_3 as supports. *Catalysts* **2015**, *5*, 1872–1896. [CrossRef]
33. Idriss, H.; Scott, M.; Llorca, J.; Chan, S.C.; Chiu, W.; Sheng, P.-Y.; Yee, A.; Blackford, M.A.; Pas, S.J.; Hill, A.J.; et al. A phenomenological study of the metal-oxide interface: The role of catalysis in hydrogen production from renewable resources. *ChemSusChem* **2008**, *1*, 905–910. [CrossRef] [PubMed]
34. Kaila, R.K.; Gutiérrez, A.; Slioor, R.; Kemell, M.; Leskelä, M.; Krause, A.O.I. Zirconia-supported bimetallic RhPt catalysts: Characterization and testing in autothermal reforming of simulated gasoline. *Appl. Catal. B* **2008**, *84*, 223–232. [CrossRef]
35. Song, H.; Ozkan, U.S. Economic analysis of hydrogen production through a bio-ethanol steam reforming process: Sensitivity analyses and cost estimations. *Int. J. Hydrogen Energy* **2010**, *35*, 127–134. [CrossRef]
36. Myers, R.H.; Montgomery, D.C.; Anderson-Cook, C.M. *Response Surface Methodology: Process and Product Optimization Using Designed Experiments*; John Wiley & Sons: Hoboken, NJ, USA, 2009.
37. Cifuentes, B.; Hernández, M.; Monsalve, S.; Cobo, M. Hydrogen production by steam reforming of ethanol on a RhPt/CeO_2/SiO_2 catalyst: Synergistic effect of the Si:Ce ratio on the catalyst performance. *Appl. Catal. A* **2016**, *523*, 283–293. [CrossRef]
38. Geravand, E.; Shariatinia, Z.; Yaripour, F.; Sahebdelfar, S. Synthesis of copper–silica nanosized catalysts for 2-butanol dehydrogenation and optimization of preparation parameters by response surface method. *Chem. Eng. Res. Des.* **2015**, *96*, 63–77. [CrossRef]
39. Rossetti, I.; Compagnoni, M.; Torli, M. Process simulation and optimization of H_2 production from ethanol steam reforming and its use in fuel cells. 2. Process analysis and optimization. *Chem. Eng. J.* **2015**, *281*, 1036–1044. [CrossRef]
40. Ye, G.; Xie, D.; Qiao, W.; Grace, J.R.; Lim, C.J. Modeling of fluidized bed membrane reactors for hydrogen production from steam methane reforming with Aspen Plus. *Int. J. Hydrogen Energy* **2009**, *34*, 4755–4762. [CrossRef]
41. Chang, H.; Liau, J.-S.; Ho, C.-D.; Wang, W.-H. Simulation of membrane distillation modules for desalination by developing user's model on Aspen Plus platform. *Desalination* **2009**, *249*, 380–387. [CrossRef]
42. Sangal, V.; Kumar, V.; Mishra, M. Optimization of a divided wall column for the separation of C4-C6 normal paraffin mixture using Box-Behnken design. *Chem. Ind. Chem. Eng. Q.* **2013**, *19*, 107–119. [CrossRef]
43. Hou, T.; Yu, B.; Zhang, S.; Xu, T.; Wang, D.; Cai, W. Hydrogen production from ethanol steam reforming over Rh/CeO_2 catalyst. *Catal. Commun.* **2015**, *58*, 137–140. [CrossRef]
44. Auprêtre, F.; Descorme, C.; Duprez, D. Bio-ethanol catalytic steam reforming over supported metal catalysts. *Catal. Commun.* **2002**, *3*, 263–267. [CrossRef]
45. Kalamaras, C.M.; Petallidou, K.C.; Efstathiou, A.M. The effect of La^{3+}-doping of CeO_2 support on the water-gas shift reaction mechanism and kinetics over Pt/$Ce_{1-x}La_xO_{2-\delta}$. *Appl. Catal. B* **2013**, *136–137*, 225–238. [CrossRef]
46. Scarabello, A.; Dalle Nogare, D.; Canu, P.; Lanza, R. Partial oxidation of methane on Rh/ZrO_2 and Rh/Ce–ZrO_2 on monoliths: Catalyst restructuring at reaction conditions. *Appl. Catal. B* **2015**, *174–175*, 308–322. [CrossRef]
47. Jakdetchai, O.; Nakajima, T. Mechanism of the water–gas shift reaction over Cu(110), Cu(111) and Cu(100) surfaces: An AM1-d study. *J. Mol. Struct. THEOCHEM* **2002**, *619*, 51–58. [CrossRef]
48. Diagne, C.; Idriss, H.; Kiennemann, A. Hydrogen production by ethanol reforming over Rh/CeO_2–ZrO_2 catalysts. *Catal. Commun.* **2002**, *3*, 565–571. [CrossRef]
49. Silva, A.M.; Costa, L.O.O.; Barandas, A.P.M.G.; Borges, L.E.P.; Mattos, L.V.; Noronha, F.B. Effect of the metal nature on the reaction mechanism of the partial oxidation of ethanol over CeO_2-supported Pt and Rh catalysts. *Catal. Today* **2008**, *133–135*, 755–761. [CrossRef]

50. Liu, H.-H.; Wang, Y.; Jia, A.-P.; Wang, S.-Y.; Luo, M.-F.; Lu, J.-Q. Oxygen vacancy promoted CO oxidation over Pt/CeO_2 catalysts: A reaction at Pt–CeO_2 interface. *Appl. Surf. Sci.* **2014**, *314*, 725–734. [CrossRef]
51. Diagne, C.; Idriss, H.; Pearson, K.; Gómez-García, M.A.; Kiennemann, A. Efficient hydrogen production by ethanol reforming over Rh catalysts. Effect of addition of Zr on CeO_2 for the oxidation of CO to CO_2. *Comptes Rendus Chim.* **2004**, *7*, 617–622. [CrossRef]
52. Cavallaro, S. Ethanol steam reforming on Rh/Al_2O_3 catalysts. *Energy Fuels* **2000**, *14*, 1195–1199. [CrossRef]
53. Martínez-Arias, A.; Hungría, A.B.; Munuera, G.; Gamarra, D. Preferential oxidation of CO in rich H_2 over CuO/CeO_2: Details of selectivity and deactivation under the reactant stream. *Appl. Catal. B* **2006**, *65*, 207–216. [CrossRef]
54. Llera, I.; Mas, V.; Bergamini, M.L.; Laborde, M.; Amadeo, N. Bio-ethanol steam reforming on Ni based catalyst. Kinetic study. *Chem. Eng. Sci.* **2012**, *71*, 356–366. [CrossRef]
55. Munera, J.; Irusta, S.; Cornaglia, L.; Lombardo, E.; Vargascesar, D.; Schmal, M. Kinetics and reaction pathway of the CO_2 reforming of methane on Rh supported on lanthanum-based solid. *J. Catal.* **2007**, *245*, 25–34. [CrossRef]
56. da Silva, A.M.; de Souza, K.R.; Jacobs, G.; Graham, U.M.; Davis, B.H.; Mattos, L.V.; Noronha, F.B. Steam and CO_2 reforming of ethanol over Rh/CeO_2 catalyst. *Appl. Catal. B* **2011**, *102*, 94–109. [CrossRef]
57. Yee, A.; Morrison, S.; Idriss, H. The reactions of ethanol over M/CeO_2 catalysts. *Catal. Today* **2000**, *63*, 327–335. [CrossRef]
58. Hou, T.; Zhang, S.; Chen, Y.; Wang, D.; Cai, W. Hydrogen production from ethanol reforming: Catalysts and reaction mechanism. *Renew. Sustain. Energy Rev.* **2015**, *44*, 132–148. [CrossRef]
59. Özkara-Aydınoğlu, Ş.; Özensoy, E.; Aksoylu, A.E. The effect of impregnation strategy on methane dry reforming activity of Ce promoted Pt/ZrO_2. *Int. J. Hydrogen Energy* **2009**, *34*, 9711–9722. [CrossRef]
60. Yu, C.Y.; Lee, D.W.; Park, S.J.; Lee, K.Y.; Lee, K.H. Study on a catalytic membrane reactor for hydrogen production from ethanol steam reforming. *Int. J. Hydrogen Energy* **2009**, *34*, 2947–2954. [CrossRef]
61. Ciambelli, P.; Palma, V.; Ruggiero, A. Low temperature catalytic steam reforming of ethanol. 2. Preliminary kinetic investigation of Pt/CeO_2 catalysts. *Appl. Catal. B* **2010**, *96*, 190–197. [CrossRef]
62. Zanchet, D.; Santos, J.B.O.; Damyanova, S.; Gallo, J.M.R.; Bueno, J.M.C. Toward understanding metal-catalyzed ethanol reforming. *ACS Catal.* **2015**, *5*, 3841–3863. [CrossRef]
63. Anderson, M.J.; Whitcomb, P.J.; Shari, L.K.; Adams, W. *Handbook for Experimenters*; Stat-Ease, Inc.: Minneapoliscity, MN, USA, 2009.
64. Lopes, D.G.; da Silva, E.P.; Pinto, C.S.; Neves, N.P.; Camargo, J.C.; Ferreira, P.F.P.; Furlan, A.L.; Lopes, D.G. Technical and economic analysis of a power supply system based on ethanol reforming and PEMFC. *Renew. Energy* **2012**, *45*, 205–212. [CrossRef]
65. Liao, X.; Chu, W.; Dai, X.; Pitchon, V. Bimetallic Au-Cu supported on ceria for PROX reaction: Effects of Cu/Au atomic ratios and thermal pretreatments. *Appl. Catal. B* **2013**, *142–143*, 25–37. [CrossRef]
66. Grande, C.A.; Lopes, F.V.S.; Ribeiro, A.M.; Loureiro, J.M.; Rodrigues, A.E. Adsorption of off-gases from steam methane reforming (H_2, CO_2, CH_4, CO and N_2) on activated carbon. *Sep. Sci. Technol.* **2008**, *43*, 1338–1364. [CrossRef]
67. Hernández, L.; Kafarov, V. Use of bioethanol for sustainable electrical energy production. *Int. J. Hydrogen Energy* **2009**, *34*, 7041–7050. [CrossRef]
68. Elmer, T.; Worall, M.; Wu, S.; Riffat, S.B. Fuel cell technology for domestic built environment applications: State of-the-art review. *Renew. Sustain. Energy Rev.* **2015**, *42*, 913–931. [CrossRef]
69. Martavaltzi, C.S.; Pampaka, E.P.; Korkakaki, E.S.; Lemonidou, A.A. Hydrogen production via steam reforming of methane with simultaneous CO_2 capture over $CaO-Ca_{12}Al_{14}O_{33}$. *Energy Fuels* **2010**, *24*, 2589–2595. [CrossRef]
70. Rydén, M.; Ramos, P. H_2 production with CO_2 capture by sorption enhanced chemical-looping reforming using NiO as oxygen carrier and CaO as CO_2 sorbent. *Fuel Process. Technol.* **2012**, *96*, 27–36. [CrossRef]
71. Ogo, S.; Shimizu, T.; Nakazawa, Y.; Mukawa, K.; Mukai, D.; Sekine, Y. Steam reforming of ethanol over K promoted Co catalyst. *Appl. Catal. A* **2015**, *495*, 30–38. [CrossRef]
72. Freni, S.; Maggio, G.; Cavallaro, S. Ethanol steam reforming in a molten carbonate fuel cell: A thermodynamic approach. *J. Power Sources* **1996**, *62*, 67–73. [CrossRef]

73. Sanchez, N.; Ruiz, R.Y.; Cifuentes, B.; Cobo, M. Hydrogen from glucose: A combined study of glucose fermentation, bioethanol purification, and catalytic steam reforming. *Int. J. Hydrogen Energy* **2016**, *41*, 5640–5651. [CrossRef]
74. Ghelamallah, M.; Granger, P. Supported-induced effect on the catalytic properties of Rh and Pt-Rh particles deposited on La_2O_3 and mixed α-Al_2O_3-La_2O_3 in the dry reforming of methane. *Appl. Catal. A* **2014**, *485*, 172–180. [CrossRef]
75. Mondal, T.; Pant, K.K.; Dalai, A.K. Catalytic oxidative steam reforming of bio-ethanol for hydrogen production over Rh promoted Ni/CeO_2–ZrO_2 catalyst. *Int. J. Hydrogen Energy* **2015**, *40*, 2529–2544. [CrossRef]
76. Ferreira, S.L.C.; Bruns, R.E.; da Silva, E.G.P.; Dos Santos, W.N.L.; Quintella, C.M.; David, J.M.; de Andrade, J.B.; Breitkreitz, M.C.; Jardim, I.C.S.F.; Neto, B.B. Statistical designs and response surface techniques for the optimization of chromatographic systems. *J. Chromatogr. A* **2007**, *1158*, 2–14. [CrossRef] [PubMed]
77. Adams, T.A.; Barton, P.I. Combining coal gasification and natural gas reforming for efficient polygeneration. *Fuel Process. Technol.* **2011**, *92*, 639–655. [CrossRef]